Physical understanding of the tropical cyclone intensity and size relations over the North Indian Ocean

Yerni Srinivas Nekkali[1] · Krishna Kishore Osuri[1] · M. Mohapatra[2]

Abstract

Tropical cyclone (TC) size and intensity define the potential destructiveness in the land-falling region. This study investigates the inter-relationships between size parameters (radius of maximum wind, R_{max}; 34-knots wind, R34; and TC-fullness, TCF) and intensity. The best-track (size and intensity) data is obtained from the Joint Typhoon Warning Center during 2002–2021. The frequently observed R34, R_{max}, and TCF are 100–150 km, 20–60 km, and 0.8, respectively for NIO TCs. Intensity and TCF are more strongly related (0.7) than R34 (0.5) and R_{max} (0.6). Analysis shows that size changes are weakly related to intensity changes (0.37–0.39). Diagnostic analysis has been conducted to address possible reasons for different TC groups 1) TCs with no size variation with intensity (Group-1), (2) both increase (Group-2), (3) size increases with no intensity change (Group-3), (4) Initial more size (Group-4). The dry air intrusion outside the eyewall in Group-1 TCs in low vertical wind shear condition limit rain-bands development, enabling moisture convergence into the primary eyewall that helps maintain storm intensity without R34 increase. Strong surface fluxes in the primary eyewall region support convection and absolute angular momentum (AAM) at upper and lower levels, which boosts size and intensity in Group-2 TCs. Strong and broader surface fluxes and vertical velocities may create rain-bands or secondary-eyewall, causing bigger TCs with limited intensification in Group-3 TCs. Larger initial TC vortices maintain wider and intense surface fluxes, vertical velocities, and AAM in the TC inner and outer cores, supporting the maintenance of larger TC size in Group-4.

Keywords Tropical cyclones · Size · Fullness · Intensity · North Indian Ocean · Physical processes

1 Introduction

The potential destruction due to storm surges, uneven distribution of strong wind, heavy rain, etc., associated with tropical cyclones (TCs) in the coastal regions depends on their intensity and size (Irish et al. 2008; Li et al. 2019). The intensity refers to the maximum sustained wind speed (V_{max}) of the TC, while the size is a measure of the radial expansion/structure of the wind field from the TC center (Knaff et al. 2007; Nekkali et al. 2022a, b). There are different metrics to indicate the TC size. The radius of maximum wind (R_{max}), the radius of 34 knots (R34), 50 knots (R50), 64 knots (R64), and the radius of outermost closed isobars

(ROCI), etc. have been widely used as TC size parameters (Knaff et al. 2007). Previous research demonstrates the decrease in R_{max} and increases in the average size of the TC (measured in terms of R34, R50, and R64) with intensity (Mohapatra and Sharma 2015; Nekkali et al. 2022a). Nekkali et al. (2022a) also demonstrated that the TCs exhibit large variations in TC size at a particular intensity stage. For instance, the R34, R50, and R64 range between 80–250 km, 25–150 km, and 20–70 km, respectively, at severe cyclonic intensity stage over the north Indian Ocean (NIO) (Nekkali et al. 2022a).

Many studies have shown that the size and intensity relationship over the global oceans and the plausible reasons/factors influencing that. Previous studies concluded that the TCs with a small inner core (R_{max} as a measure) and/or large outer core (R34 as a measure) favor the TC intensification (Wu et al. 2015). Merrill (1984) observed a weak correlation (0.26) between V_{max} (intensity parameter) and ROCI (size parameter) for Western North Pacific and Atlantic TCs during 1961–1969 and 1957–1977, respectively. Similarly, a

✉ Krishna Kishore Osuri
osurikishore@gmail.com

1 Department of Earth and Atmospheric Sciences, NIT Rourkela, Rourkela, Odisha, India

2 India Meteorological Department, New Delhi, India

recent study by Guo and Tan (2017) also finds a weak correlation (0.29) between the size parameter (R34) and intensity of TCs over the Atlantic Ocean for the period 1988–2015. On the other hand, Song et al. (2020) demonstrated that the strong and long-lived TCs exhibit a linear relation between size and intensity as compared to weak, short-life, and recurving TCs. Later, the intensity and R_{max} size are observed to have a robust correlation (0.6), which is significantly stronger than in other/earlier investigations (Ruan and Wu 2022). Note that a substantial connection (≥ 0.6) is seen during the development stages of individual TCs between intensity and size (Chen et al. 2021). In addition, Guo and Tan (2017) found a significant correlation (~ 0.7) between intensity and combined size parameters, known as tropical cyclone fullness (TCF) rather than using any one particular size parameter.

Recent years have witnessed different TC sizes corresponding to a particular intensity. For example, very severe cyclone Yaas (2021) has a larger size (~ 270 km) at the CS stage, whereas it is ~ 100 km for the Super cyclone Amphan (2020) at the same intensity over the NIO region. It suggests that the relationship between size and intensity is not linear and depends on dynamical and thermo-dynamical processes in the inner-core and environmental processes (Wang 2009; Hill and Lackmann 2009; Xu and Wang 2010; Chan and Chan 2013; Nekkali et al. 2022a). For instance, Wang (2009) and Nekkali et al. (2022a) found that the rain-band region's diabatic heating is advantageous for TC size expansion while suppressing intensity. The saturated (unsaturated) moisture conditions in the outer core region encourage size enlargement (reduction) and intensity suppression (enhancement). Chan and Chan (2013) observed that the size (intensity) of the TCs depends on the angular momentum transport in the lower (upper) atmosphere. Similarly, Tao and Zhang (2019) have observed a positive effect of wind shear on size and a negative effect on intensity. Moreover, Xu and Wang (2018b) observed that the intensification rate is proportional to sea surface temperature (SST) and it accounts for the change in TC size (Lin et al. 2015; Busireddy et al. 2022).

Realizing the importance of the TC intensity and size on destruction in the coastal regions of NIO basin, India Meteorological Department (IMD) has been providing the real time size information since 2010 (Mohapatra 2014). Previous studies on the NIO have shown that the initial sea surface temperature influences the TC intensity and size (Busireddy et al. 2022; Nadimpalli et al. 2023). In addition, other studies conducted by Nekkali et al. (2022a, b) show that the location of heating due to microphysical processes has a substantial effect on the size and intensity changes of TCs. To the best of knowledge, the majority of studies on the NIO basin focus on the factors influencing the size and intensity separately. No comprehensive study of the relationship between them is available over this basin. Therefore,

this study focused on revealing the relationship between intensity and different size parameters and factors controlling the relationship over the NIO basin.

The rest of the paper is organized as follows: data and methodology used in the study are described in Sect. 2. Section 3 introduces the general relation between TC intensity and various parameters and possible factors that affect the size and intensity relation. The detailed summary and conclusions are presented in Sect. 4.

2 Data and methodology

2.1 Data

This study considers all the TCs formed during 2002–2021 over the NIO basin. There are 82 TCs in this period. Six hourly best track information obtained from the Joint Typhoon Warning Center (JTWC). It provides TC track (center latitude and longitude), intensity (minimum sea level pressure (MSLP) and V_{max}), and size parameters such as R_{max}, R34, R50, R64, and ROCI. Six hourly infrared (IR) brightness temperature at $0.07° \times 0.07°$ horizontal resolution is obtained from the GridSat under the International Satellite Cloud Climatological Project (ISCCP; Knapp et al. 2011). The identification of tropical disturbances and estimation of their characteristics (intensity and wind structure) using this IR brightness temperature has proven to be effective (Knapp et al. 2011). High-resolution (~ 10 km) rainfall is acquired from Global Precipitation Measurement (GPM; Huffman et al. 2019). GPM captures the spatial and temporal variation of rainfall in intense convective regions (Ma et al. 2021; Saikrishna et al. 2021). The atmospheric parameters such as U-wind, V-wind, vertical velocities, surface fluxes, relative humidity, potential vorticity, etc. are acquired from fifth-generation European Center for Medium-Range Weather Forecasts data (ERA5; Hersbach et al. 2020) available at a spatial resolution of $0.25° \times 0.25°$. This dataset has been proven in reasonably representing the intensity and structure of the TCs over the NIO basin (Malakar et al. 2020).

2.2 Methodology

Intensity of a TC refers to the maximum sustained 10-m wind speed (V_{max}). The size parameters such as R34, R50, and R64 are the maximum radius of 34 knots, 50 knots, and 64 knots winds from TC center, respectively. JTWC provides the size information in four geographical quadrants (Knaff et al. 2007). Note that the average size of four quadrants is considered in the study. R_{max} is the radius of maximum wind from the TC center. In addition to these sizes, TCF is also considered in this analysis. The TCF is the region

between R_{max} and R34, referring to strong convection and higher winds (Guo and Tan 2017).

$$\text{TC fullness (TCF)} = \frac{R34 - R_{max}}{R34}$$

In general, the R34 is always beyond/outside the Rmax (rarely equals to Rmax in case of weak TCs). Therefore, TCF is always positive (or zero).

This study considers TCs with cyclonic storms and above to investigate the size (R_{max}, R34, and TCF) relations with intensity. Note that the TC samples over the open ocean are considered in this analysis. The size parameters R50, R64, and eye diameter are not used in the study because of the fact that these parameters are available from SCS and higher intensity stages and the number of samples would be less. Note that the ROCI exhibited poor correlation (0.2) with intensity (Figure not shown) and hence is not considered in the subsequent analysis.

The study considers 12 h change to define intensity changes. Lyu et al. (2019) demonstrated that the 95th, 65th, and 15th percentile values better indicate or separate intensity changes such as Rapid Intensification (RI), Slow Intensification (SI), Neutral Intensification (NI), and weakening (W) based on 12 h intensity changes. Further, the 12 h criteria provides good number of samples. Further, Qin et al. (2016) identified that the 12 h interval is more appropriate to study size changes. Hence, the study uses 12 h size and intensity changes. Based on 12 h intensity change (ΔV_{12}), the threshold values for 95th, 65th, and 15th percentiles for the NIO TCs during 2002–2021 are 20 knots, 5 knots, and -5 knots, respectively. Therefore, the TC cases are divided as: (1) RI cases ($\Delta V_{12} \geq 20$ knots), (2) SI cases ($5 < \Delta V_{12} < 20$ knots), (3) NI cases ($-5 \leq \Delta V_{12} \leq 5$ knots) and (4) W cases ($\Delta V_{12} > -5$ knots).

The atmospheric parameters are available in latitude/longitude grids and converted to storm-relative coordinates (radial distance and azimuthal angle) at every time step. The parameters are converted to 1° azimuthal increment around the TC center and 10 km (0.1°) radial increment up to 500 km storm radius. The parameters are bi-linearly interpolated to storm-relative coordinates. Further the direction of the TC motion is shifted to coincide with the north direction (following Balachandran and Geetha 2017; Ankur et al. 2020; Nekkali et al. 2022b). Then the composites are prepared for various diagnostic fields.

3 Results

The section examines the size parameters (R34, R_{max}, and TCF) as a function of latitude and longitude, the relationship between the TC intensity and size for different intensity change groups, and associated factors influencing the relationships.

3.1 Spatial distribution of various size parameters

The relationship between intensity and size may depend on location as a function of ocean characteristics and latitude (Chan and Chan 2018; Busireddy et al. 2019), TC intensification (different stages; Mohapatra and Sharma 2015), and large-scale atmospheric conditions Hill and Lackmann 2009; Mohapatra and Sharma 2015; Shen et al. 2021, Nadimpalli et al. 2023). To explain briefly, Chan and Chan (2018) show that the TCs are smaller in size in the lower latitudes and bigger in higher latitudes. Busireddy et al. (2019) showed that the ocean heat content and barrier layer vary with latitude and longitude over the NIO basin. Therefore, this section focuses on how the TC size varies in the NIO basin including the Arabian Sea (AS) and the Bay of Bengal (BoB). The evolution of R34, R_{max}, and TC-fullness over the NIO region as a function of latitude and longitude are presented in Fig. 1. It is known that TC occurrence is higher in 10°–15° latitude and 80°–90° longitude (Nadimpalli et al. 2021) and hence it is expected stronger size variations in this region as shown in Fig. 1. R_{max} and R34 sizes vary between 20 to > 120 km and 50 to > 300 km, respectively, over this region (Fig. 1a–d). However, 100—150 km is more common (> 15%) for R34 size (Fig. 1a, b). Individual samples show the R34 as larger as > 300 km for higher intensity stages (VSCS and above). On the other hand, smaller sizes (≤ 50 km) are typically found at lower intensity (for ex., CS) stages (not shown). Similarly, most of the cyclone's inner-core size (R_{max}) is ~40 km, followed by ~20 km and ~60 km (Fig. 1c, d). The smaller R_{max} (< 20 km) sizes are mostly distributed in the Arabian Sea (Fig. 1d). The maximum R_{max} size (> 120 km) is mainly associated with the CS intensity stage. In contrast, most of the minimum R_{max} sizes ($R_{max} \leq 20$ km) are observed at higher intensity stages (SCS and above). The larger (smaller) TCF represents the more (less) area of convection between the inner core and outer core of the TC. Most TCs over this region have a TCF value of 0.8, followed by 0.6, with the average is 0.6. Strong TCF values (≥ 0.9) are primarily seen at higher intensities (VSCS and above) and lower TCF values (≤ 0.2) at lower intensities (CS).

3.2 TC size and intensity relationship

The relation between TC size parameters and intensity for all TCs, weaker TCs (maximum intensity < 64 knots, i.e. SCS stage), and stronger TCs (maximum intensity ≥ 64 knots, i.e. VSCS stage) is analyzed during 2002–2021 and is presented in Fig. 2. It is clear that the R34 (Fig. 2a–c) and TCF (Fig. 2g–i) increase with intensity in all TC intensity

Fig. 1 **a** Latitudinal and **b** longitudinal distribution of R_{max} in terms of various magnitudes. **c**, **d** For R34, **e**, **f** for TCF, respectively. Shading indicates the region of maximum frequency
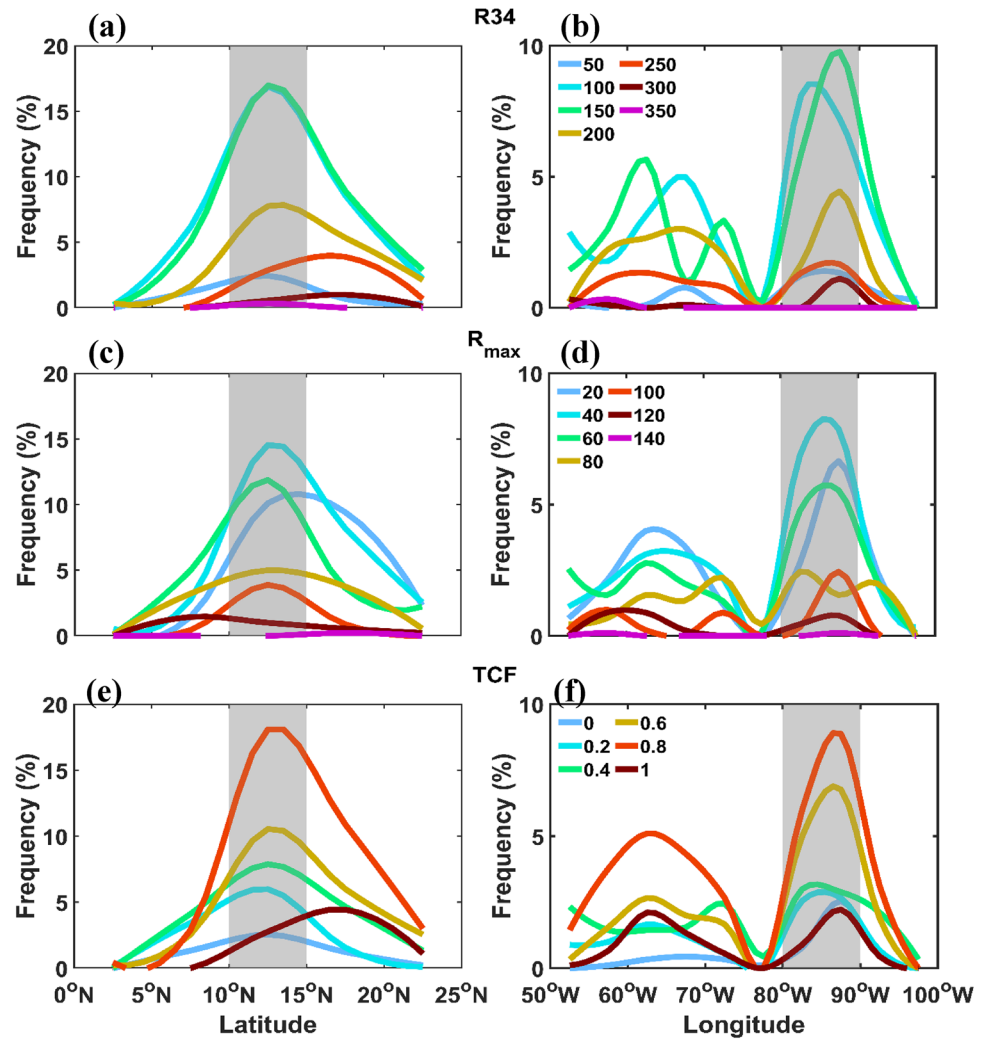
categories, whereas R_{max} decreases (Fig. 2d–f). The increase in the wind speed/intensity results into the contraction of R_{max} due to the conservation of absolute angular momentum (Holland and Merrill 1984). In this process, the diabatic heating extends to the outcore or (outside the R_{max}), favoring the convection, resulting expansion of the outer circulation and hence R34 (Kilroy et al. 2016; Nekkali et al. 2022a). Shading indicates the variation of TC size for a particular intensity stage. The TC size spreads/varies noticeably at a particular intensity, for example, the TC size at the CS stage ranges between 25 to 250 km when all TCs considered (Fig. 2a). The quadratic function fitted for size and intensity relation is represented with a black dotted line, and the equation is presented on the upper side of each subplot. The quadratic function demonstrates that a relatively linear relationship (0.5) between size and intensity is observed, with the largest average R34 size (225 km) being observed at an intensity of 140 knots (super cyclone stage) over the NIO basin (Fig. 2a; Table S1). The Western North-Pacific (WNP) basin exhibits a maximum R34 size of 400 km at

90 knots wind speed (Song et al. 2020). Unlike R34, a relatively linear relationship is observed between TCF and R_{max} with intensity up to the maximum wind speeds of 90 knots (Fig. 2d, g). The average minimum R_{max} and maximum TCF over the NIO basin are 20 km and 0.98 at 100 knots, respectively (Fig. 2d, g). The relation between the intensity and size parameter is determined by the correlation coefficient (CC) and coefficient of determination (R^2). The correlation coefficients are statistically significant at 99% (based on p-value in Table S1). Compared to R34 (CC: 0.5; R^2: 0.3), the TCF exhibited a strong correlation (CC: 0.7; R^2: 0.48) with intensity, followed by R_{max} (CC: -0.6; R^2: 0.4) (Table S1 and Table S2). A similar relationship is observed between size and intensity for weaker cyclones (Fig. 2e, h) and stronger TCs (Fig. 2f, i). The relationship is almost flat with weak correlation (CC: ~0.2) for R34 size for weaker TCs indicating similar sizes for the TCs with less intensity stages such as CS and SCS (Table S1). On the other hand, stronger TCs exhibit stronger correlations for all TC size parameters (Fig. 2c, f, i).
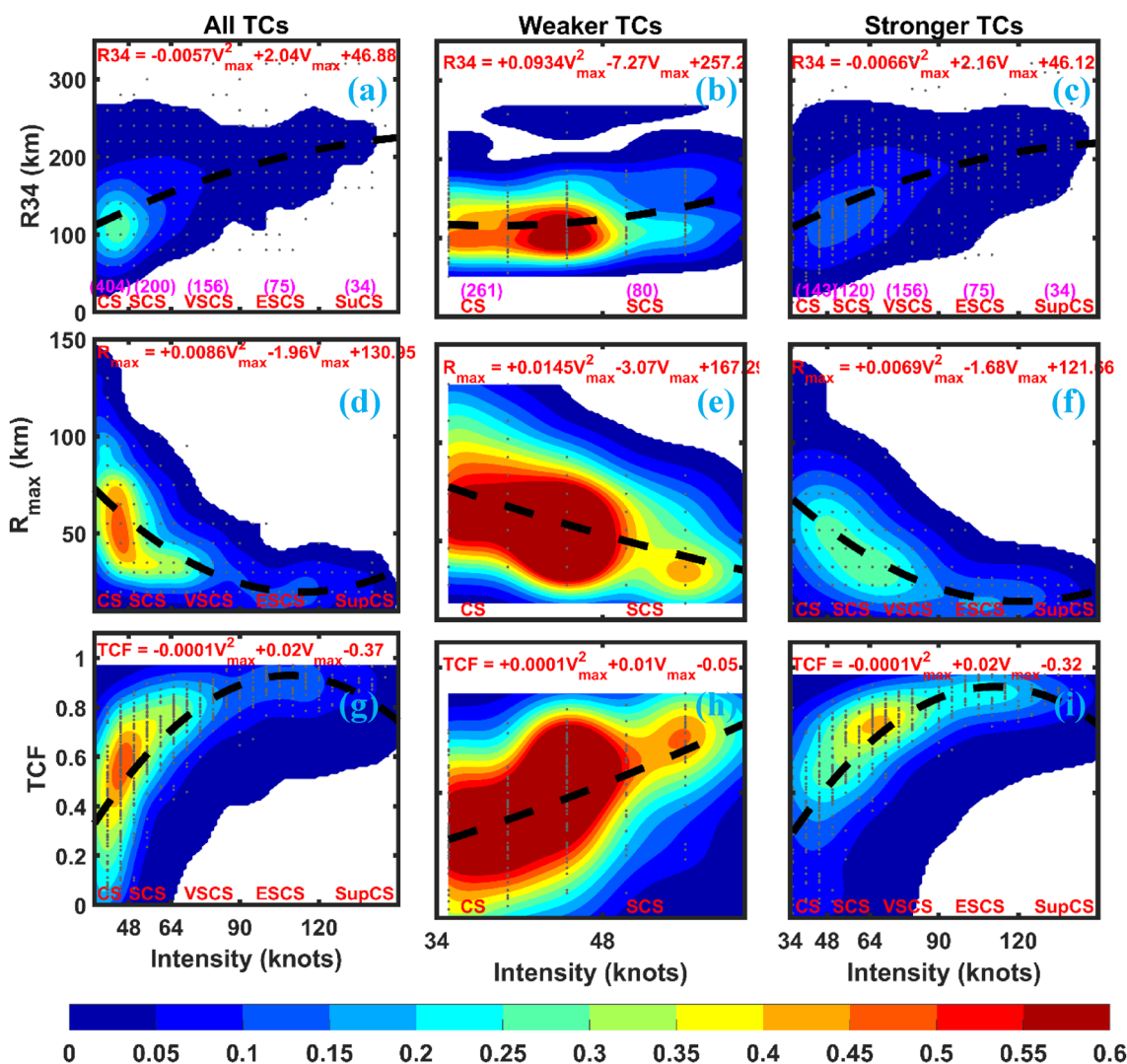
Fig. 2 Relationship between TC intensity and R34 for **a** all intensity, **b** CS + SCS, **c** VSCS and above intensity cyclones. **d–i** Are similar to **a–c** but for other R_{max} and TCF, respectively. The black dotted line represents the best-fit quadratic curve. The probability density esti-mated by using Gaussian kernel density estimation is represented by shading. The quadratic equation is presented in the upper side of each plot. Number of samples at each intensity stage are presented in parenthesis in upper panel

The frequency distribution of R34, R_{max}, and TCF for different rates of TC intensity changes in 12 h duration is presented in Fig. 3a–c. It clearly noticed that the NI and SI groups exhibit smaller R34 (~ 125 km) and larger R_{max} (≥ 40 km), hence smaller TCF values (≤ 0.7) as compared to the remaining groups (RI and W) (Fig. 3a). In contrast, RI and W groups display larger TCF values (≥ 0.7) at higher frequencies due to smaller R_{max} (≤ 30) and larger R34 (≥ 175 km). Analysis reveals that the higher TCF values related to RI and W groups are mainly due to the higher intensities (with averages of ~ 70 and ~ 80 knots respectively), while the NI and SI group's average intensity is ~ 55 knots (not shown). The analysis is further extended to study the relation between the intensity changes (ΔI_{12}) and size changes (ΔS_{12}) within 12 h period (Δ_{12}) and presented in

Fig. 3d –f. It is clear that the quadratic fitted curve between R34 and intensity changes is relatively linear, however, with less correlation (0.37). On average, R34-size changes (or decreases) by ~ 30 km when the TC is experiencing a strong weakening of ~ 30 knots and increases by ~ 50 km during a strong intensification of 60 knots (Fig. 3d). Similarly, a weak correlation is observed between intensity change and R_{max} (− 0.37)/TCF (0.39) changes (Table S3). Large spread in TC size at a particular intensity stage (refer to Fig. 2), the correlation between ΔI_{12} and ΔS_{12} is relatively weaker (Fig. 3d–f).

The analysis is further extended to address the reason for the weaker correlation between the R34 and intensity and the factors responsible for that. For this purpose, the TCs with a minimum lifetime of 48 h and achieved a
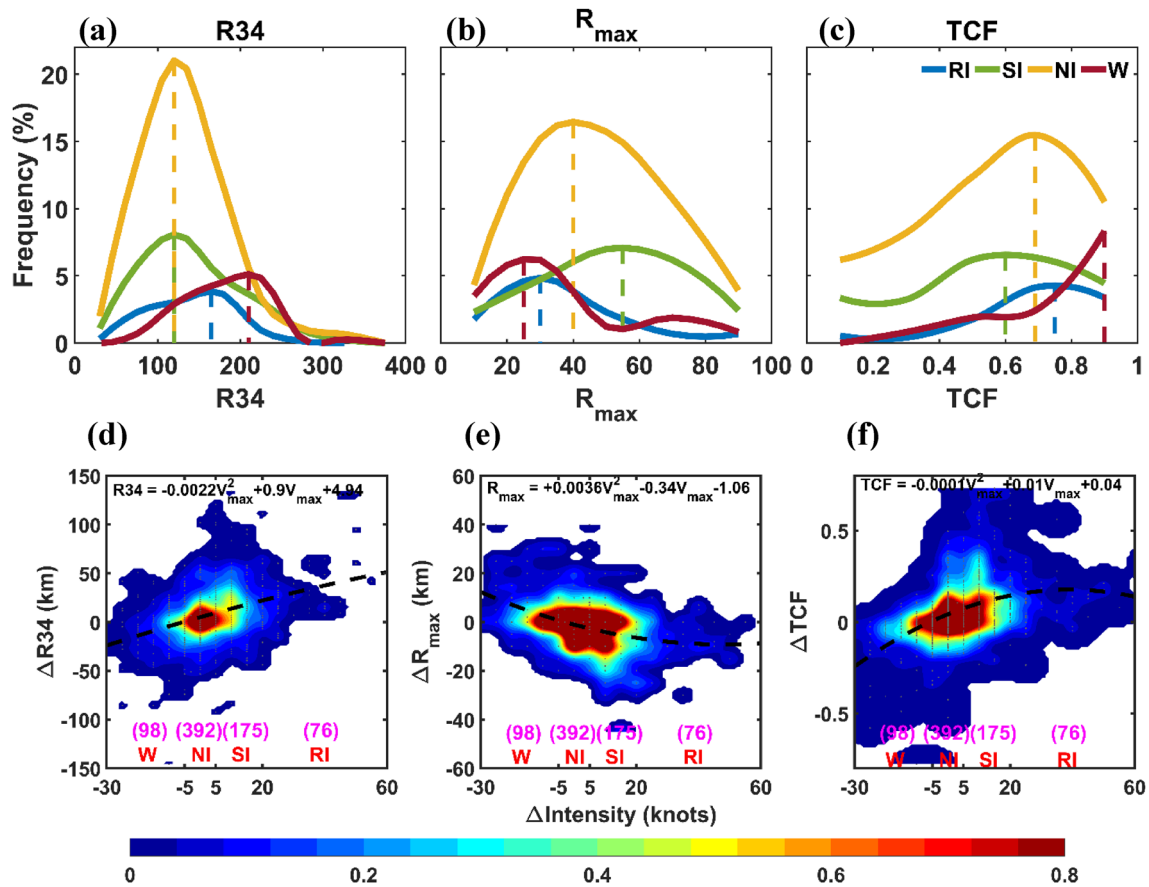
Fig. 3 Frequency distribution of size parameters **a** R34, **b** R_{max}, **c** TCF among various intensity change groups RI, SI, NI, and W. **d**–**f** Are similar to Fig. 2a–c but for respective fields changes (Δ_{12}) of in 12 h period

maximum intensity of VSCS and above in its lifetime are considered. 37 TCs over the NIO basin are considered in this analysis and categorized into four groups based on Linear Regression Coefficient (LRC) of size-intensity relation. Group–1 TCs exhibit no size variation with intensity, having $0.5 \leq LRC < 1.5$ km/knots. (2) The size of Group–2 TCs increases with intensity, showing LRC between 1.5 to 2.5 km/knots. (3) In Group–3, size increases with no or less intensity change and LRC varies between 2.5 to 3.5 km/knots. The average LRC of Group–1, Group–2, and Group–3 are 1.42 km/knots, 2.18 km/knots, and 2.7 km/knots, respectively. Another group of TCs exhibiting larger initial sizes corresponding to different initial intensities (for say, CS, SCS, VSCS, etc.) and considered into Group-4. Based on composites, the average ± 1 standard deviation (SD) of R34 sizes over the NIO at CS, SCS, and VSCS are 115 ± 45, 140 ± 48, and 170 ± 50 knots, respectively (Figure not shown). Note that the TCs with size larger than mean + 1SD are considered in Group-4. The average LRC of the Group–4 TCs is 3.62 km/knots. Note that these relations are investigated during the TC intensification period (from the initial CS stage to the maximum intensity of individual

cyclones) and weakening phase is not considered to avoid land-interactions.

Group-wise relationship between R34 and intensity for 37 TCs over the NIO basin is presented in Fig. 4. The number of TCs grouped in each category is mentioned in parenthesis. In Group-1, the average size of TC at ~ 64 knots wind speed (VSCS stage) is about 100 km. While, it is ~ 150, ~ 190, and ~ 240 km in Group-2, Group-3, and Group-4, respectively (Figure not shown). The majority of TCs (~ 50%) belong to the Group-2 (i.e. size monotonically increases with intensity), followed by Group-1 (25%). The remaining two categories Group-3 and Group-4 are 10 and 15%, respectively. Thus, this analysis shows the characteristic differences in R34 with intensity, and the possible reasons are analyzed in subsequent sections.

The scatter plot in Fig. 5 illustrates the size (R34, R_{max}, and TCF) and intensity relation during the intensification phase (initial time to peak intensity time) of above mentioned VSCS TCs. Note that the samples in the weakening phase (peak intensity to dissipation) are not considered in this analysis. It reveals that the Group-4 TCs are initially larger in R34 size and are maintained the entire life period of
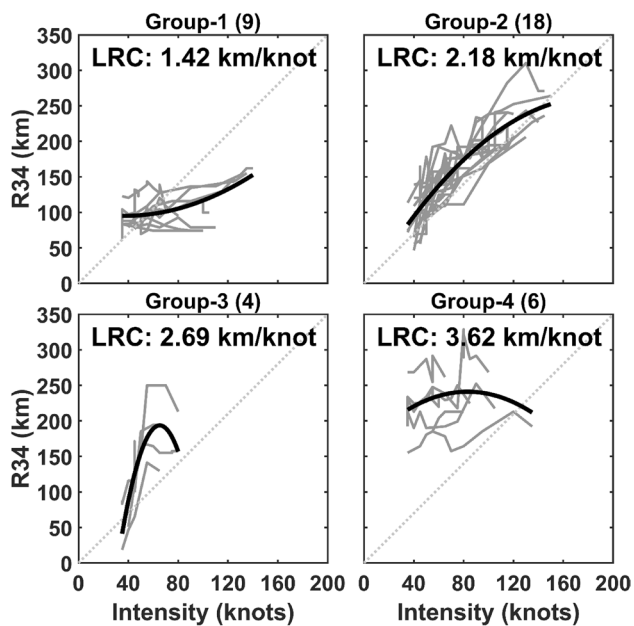
Fig. 4 Relationship of intensity and R34 of VSCS cyclones in their lifetime during 2002–2020. Based on the slopes, cyclonic are divided into 4 groups: **a** Group-1 (low slope), **b** Group-2 (medium slope), **c** Group-3 (high slope), and **d** Group-4 (more size at initial time). The regression curve of size and intensity for each category is represented with a thick black line and the mean linear regression coefficient is displayed at the top of each panel

the TC (Fig. 5a). However, other categories exhibit similar sizes at the initial period and are diverse at later stages of TC. Similar results are found in the idealized study of Chan and Chan (2014), and Xu and Wang (2018a, b). They have noticed that the initial larger vortex maintains a larger size, whereas initial smaller size TCs may not sustain as small in their lifetime. Figure 5a exhibits different relationships between intensity and R34 size among different groups. However, no such significant differences are observed for R_{max} and TCF with intensity (Fig. 5b, c). The Group-4 TCs exhibit a large R_{max} and hence higher TCF (> 0.6) in most

instances. However, lesser R34 associated with Group-1 TCs (Fig. 5a) led to smaller TCF at all intensity categories (Fig. 5c) than the remaining groups. It is interesting to note that the occurrence of these TC groups does not show any relation with the month of formation. However, these groups exhibit variations in the basin of formation (Figure S1). Most of the BoB TCs fall in Group-2 (12 out of 18) followed by Group-3 (3 out of 4). In contrast, most of Group-1 (6 out of 9) and Group-4 TCs (4 out of 6) are formed over the AS (Figure S1).

3.3 Diagnostic analysis to understand size-intensity relationship

The convection and rainfall evolution in the radial direction of a TC exhibit distinct structural differences among these categories (Supplementary Figure S2). Note that the composites of convection (IR brightness temperature) and rainfall are prepared for different intensity stages of stronger TCs. According to Meenu et al. (2010), the convection is deep if the BT is less than 235 K and very deep if it is < 210 K. It is noticed that the deep to very deep convection prevails in the inner core in all the groups which increases with TC intensification (Figure S2a–c) and is consistent with previous studies. In Group-1 TCs, very-deep convection (< 210 K) is located in the TC inner core (100 km) for each intensity stage. However, the convection has reduced (> 240 K) radially outwards in Group-1 TCs compared to the remaining groups (Figure S2a–c). Inner core convection is relatively weaker (by 10 K) in Group-3 and Group-4 at the CS stage compared to Group-1 and Group-2 (Figure S2a). While, relatively stronger convection (~5 K) is seen in Group-3 TCs beyond the inner-core (Figure S2a, b). At the VSCS stage, unlike Group-1, the remaining groups exhibit similar convective profiles radially (Figure S2c).

The primary and secondary circulations such as tangential and radial winds, vertical velocities, and absolute angular momentum (AAM), etc. impacts intensity and size
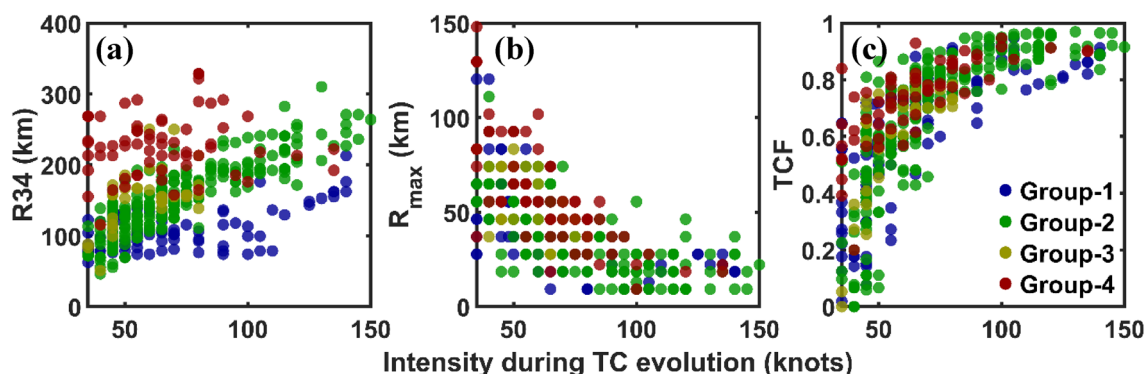
Fig. 5 TC size variations with intensity in TC lifetime from all the groups for **a** R34, **b** V_{max}, **c** TCF

(Wang 2009; Ying and Zhang 2012; Chan and Chan 2013). Therefore, the evolution of these circulations are analyzed to address the possible reasons for size-intensity relationship. The azimuthally averaged radial (V_r) and tangential (V_t) winds for the above-mentioned four groups of TCs at different intensity stages are presented in Fig. 6. Both the circulations increase with intensity in all the groups (refer to column-wise subplots of Fig. 6). In addition, the R_{max} (blue line) moving inwards with intensity increase (CS to VSCS), mainly in the lower-levels. The basic structure, i.e., the maximum tangential wind attains above the boundary layer and reduce magnitude with height, however, shows noticeable variations in vertical and azimuthal direction for different intensity groups (for ex., Fig. 6a–d). The tangential wind has been broadening in radial direction from Group-1 to Group-4. Consistent with the smaller sizes in Group-1, tangential wind speed is very low and confined to a small area as compared to the remaining groups. For example, the 15 m s^{-1} wind is mostly confined within 200 km in Group-1. Whereas for other groups it varies 300–500 km. Similarly, the radial wind related to Group-1 is sallower and less (2 m s^{-1}) (Fig. 6a, e, i). While Group-2 TCs exhibit outward wedge-shaped tangential wind distribution, and vertically extended to higher levels as compared to the remaining (Fig. 6b, f, j). Such evolution in these circulations supports and serves as a better indicator of TC intensification (Qi et al. 2018). In Group-3, the tangential wind field is broader but confined to the lower to middle troposphere mostly. Whereas strong and broader radial and tangential winds are observed in the Group-4 TCs (Fig. 6d, h, l). The broadening of tangential wind leads to the development of the subsequent secondary tangential wind maximum and hence increases in size of tropical cyclones (Abarca and Montgomery 2013). It is interesting to note that the radial winds
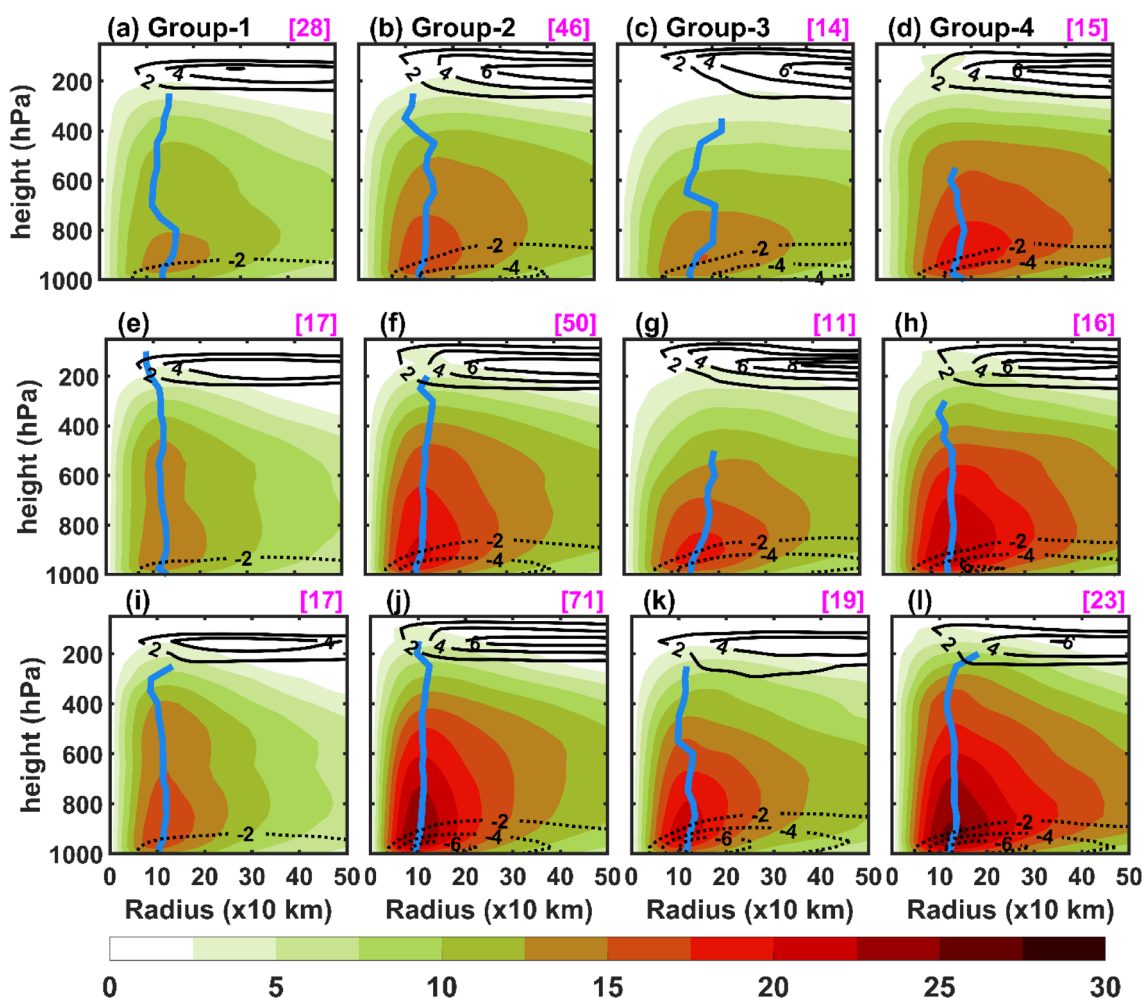
Fig. 6 Azimuthally averaged tangential (shading; ms^{-1}) and radial winds (contours; m s^{-1}) of **a** Group-1, **b** Group-2, **c** Group-3, and **d** Group-4 cyclones during at a cyclone (CS) intensity stage. **e–l** Is similar to **a–d** but for the SCS and VSCS stages. Note that the green line indicates the vertical profile of the radius of maximum wind. Number in square bracket in top of each subplot represents the number of samples

increase with intensity in Group-2 to Group-4 in which the TC size varies with intensity (columns 2–4 of Fig. 6). There exist differences in the areal extent of radial wind. For example, intense inflow (4 m s^{-1}) prevails up to 400 km in Group-2, whereas it is ~450 to 500 km in Group-3 and Group-4.

The azimuthally averaged AAM and vertical velocity (Pa s^{-1}) are presented in Fig. 7. With TC intensification, the gradient of AAM has been enhanced in the primary eyewall region. For example, the AAM gradient within a 100 km radius is less than 15×10^5 m s^{-2} at each intensity stage of Group-1 TCs, with a $2–3 \times 10^5$ m s^{-2} increase between the intensity stages (Fig. 7a, e, i). The respective values in Group-2 TCs are in between $15–25 \times 10^5$ m s^{-2} within a 100 km radius, showing ~5×10^5 m s^{-2} increase between the stages (Fig. 7b, f, j). The Group-3 TCs exhibit slant and weaker AAM in the upper level than the other groups, however, an increase in the lower AAM is noticed as that in other groups. A study by Chan and Chan (2013) also concluded that strong AAM in the lower (upper) troposphere favors the TC size (intensity). From initial intensity, stronger AAM is

observed in the Group-4 TCs within and outside the eyewall region (Fig. 7d, h, l) than in other group TCs. The larger initial vortex supports a strong AAM gradient in the rain-band region (200–400 km), favorable to maintaining a larger size (Chan and Chan 2014, 2015). Like AAM, the Group-1 TCs exhibit lower vertical velocities (0.7 Pa s^{-1}) than the remaining groups. While the strong vertical velocities are associated with Group-2 and are mostly confined within R_{max}. In Group-1 and Group-2, the alignment of AAM and vertical velocities in the primary eyewall region indicates less wind shear (refer to Supplementary Figure S3). Whereas in Group-3 and Group-4, vertical velocities are weak, widely spread and slant in nature mostly in CS and SCS intensity stages as compared to Group-2 (Fig. 7c, d, g, h).

The previous modeling and observational studies have identified the dependency of size and intensity on large-scale environmental processes such as surface fluxes, relative humidity, and potential vorticity (Hill and Lackmann 2009; Xu and Wang 2010; Shen et al. 2021; Nekkali et al. 2022a, b; Busireddy et al. 2022; Nadimpalli et al. 2023). The plane
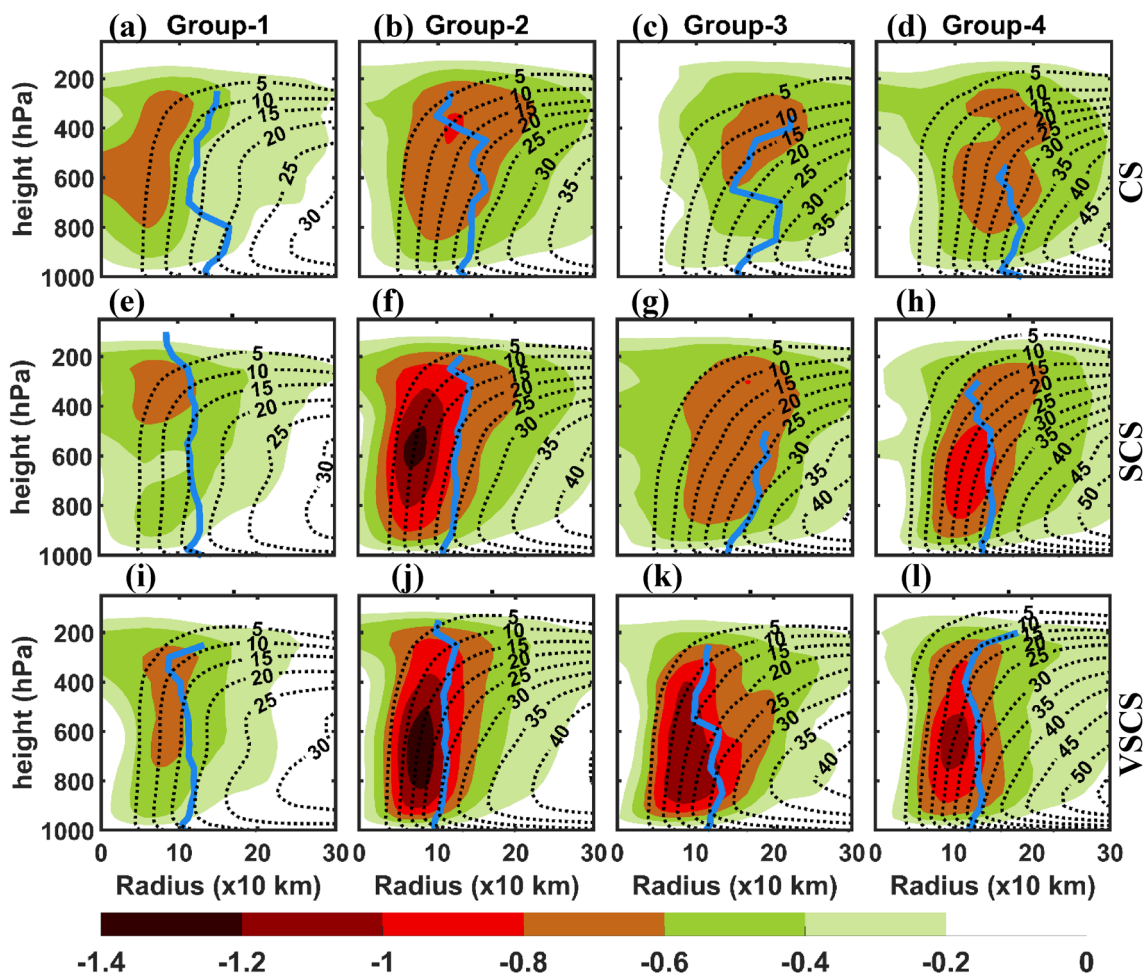

Fig. 7 Similar to Fig. 6 but for vertical velocities (shading; Pa s^{-1}) and Absolute angular momentum (contours; $\times 10^5$ m s^{-2})

view of the average surface fluxes such as a surface latent heat flux (LHF) and sensible heat flues (SHF) anomalies for these TC groups at different intensity stages are presented in Fig. 8. Note that the anomalies are determined by the deviation of fluxes during the TC period to the average fluxes 15 days prior to TC formation. Overall, the intensification of TCs (from CS to VSCS) shows a positive relation with SHF and LHF for each TC group. During Group-1 TC intensification (CS to VSCS), the increments in LHF (50 W m^{-2}) and SHF (5 W m^{-2}) are the least (Fig. 8a, e, i). Significant increments (~ 150 W m^{-2} LHF and > 10 W m^{-2} of SHF) are observed in the remaining category's evolution (Fig. 8). However, for the same intensity, the radial distribution and magnitude of fluxes vary between TC in Group-1 to Group-4. The average increment of SHF and LHF are 5 ± 2 W m^{-2}, and 100 ± 20 W m^{-2}, respectively from Group-1 to Group-4 for any particular intensity (row-wise of Fig. 8). For example, the average LHF (SHF) for Group-1 TCs at the CS stage is 30 W m^{-2} (10 W m^{-2}). While they are 120 W m^{-2} (17 W

m^{-2}) for Group-4 cyclones (Fig. 8a–d). Similarly, the radial expansion of surface fluxes has increased from Group-1 to Group-4. For example, 100 W m^{-2} of LHF is not displayed in Group-1 at the CS stage, whereas it is horizontally extended up to 250, 350, and > 450 km in Group-2, Group-3, and group-4 at the CS stage, respectively (Fig. 8a–d). Similarly, SHF of 20 W m^{-2} is confined inside the 200 km radius in Group-1 TCs. Whereas, it is extended upto 400 km in Group-4. Similar increase in the spatial extent of surface fluxes from Group-1 and Group-4 are observed for other intensity stages (SCS and VSCS) (Fig. 8e-l). According to Shen et al. (2021), the larger areal extent of fluxes in the eyewall as well as outside the eyewall (as seen in Group-3 and Group-4) favors the development of the secondary eyewall or strong rain bands promoting the formation of the secondary maximum wind field. This enhances the AAM at outside the primary eyewall region, and hence the size increases and restricts the intensification (Wang 2009; Chan and Chan 2013).
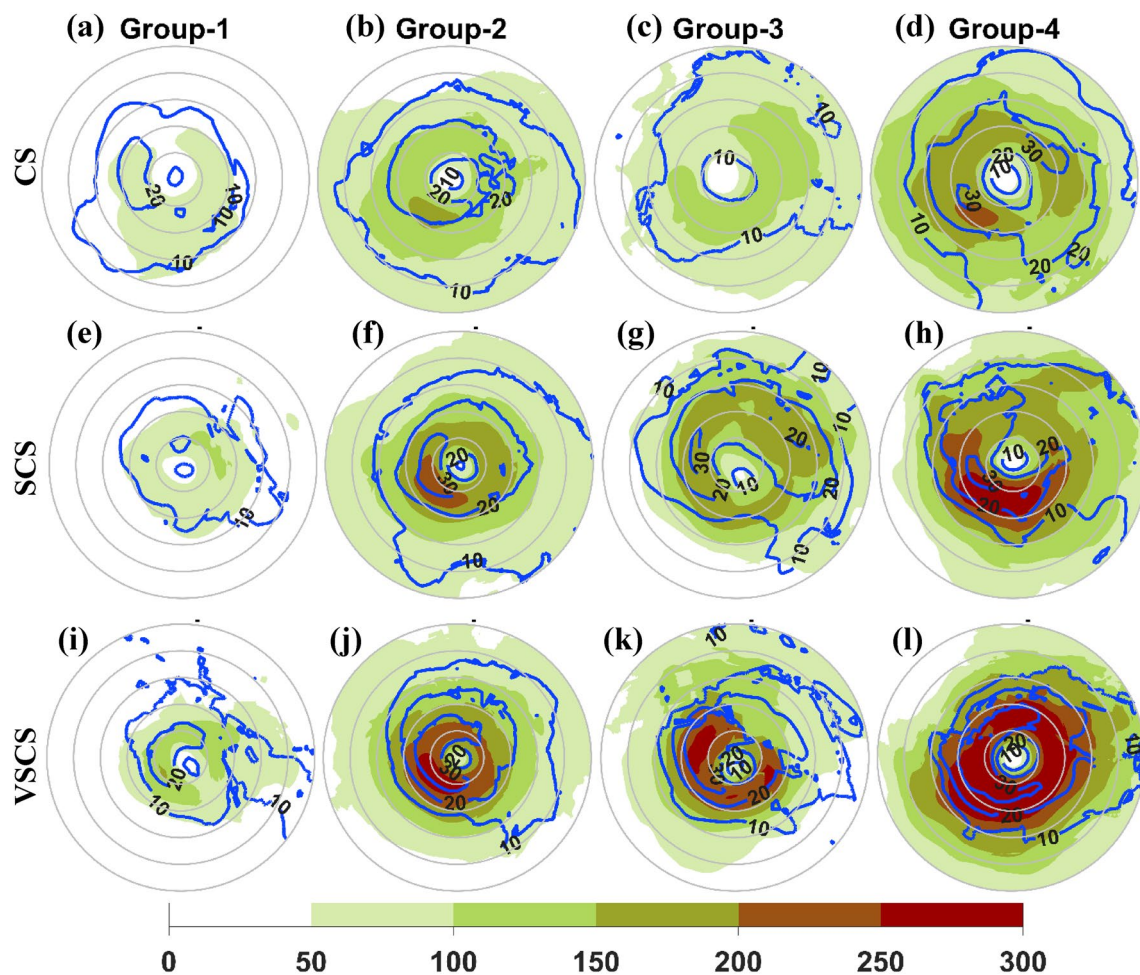
Fig. 8 Plainview of surface latent heat flux (shading; W m^{-2}) and sensible heat flux (contour; W m^{-2}) of various categories **a** Group-1, **b** Group-2, **c** Group-3 and **d** Group-4 at CS stage. **e–l** Is similar to **a**, **b** but at the SCS and VSCS stages

Azimuthally averaged relative humidity (RH) and potential vorticity (PV) corresponding to the TC groups are presented in Fig. 9. It is established in earlier studies that the enhancement of PV in the lower and upper troposphere is favorable for TC intensification (Hill and Lackmann 2009; Nekkali et al. 2022a, b). Therefore, this analysis is focused to note the characteristic changes in PV and RH profiles in connection with size-intensity changes. Increments in PV are seen in each TC group during their intensification from CS to VSCS stages (column-wise of Fig. 9). In Group-2 TCs, the humid environment (Fig. 9b, f, j) and strong surface fluxes (as shown in Fig. 8) in the primary eyewall region could be some of the factors that support the maintenance of size and intensity relation. Similarly, Group-3 TCs also exhibit relatively higher humidity saturation extended to longer radial distances (Fig. 9c, g, k). The spatial extent of surface fluxes in Group-3 TCs is more than in Group-2 TCs. These factors along with higher convection in the outer core (Figure S2) may be responsible for expansion of PV

circulation in Group-3,, hence higher R34 sizes in the presence of no-intensity or smaller-intensity changes (Fig. 9c, g, k).. In Group-4 TCs, a higher moist environment at all intensity stages (Fig. 9d, h, l) along with strong surface fluxes with more spatial extent (Fig. 8d, h, l) could promote the larger size at all intensity stages as compared to the remaining TC groups. Note that relatively, wider PV is associated with Group-4 TCs than the remaining groups. Conversely, Group-1 TCs maintain a smaller size with intensification mainly due to dry air intrusion in the upper levels (Fig. 9a, e, i) and smaller areal extent of fluxes (Fig. 8a, e, i). The dry air present outside the eyewall region suppresses the formation of rainbands. Suppression of the rainband formation leads to relatively narrower PV due to limited secondary eyewall formation and thus inhibiting the TC size. However, the TC intensification could be maintained due to relatively moist conditions in the lower troposphere of the inner core. In drier environments, TC size maintains a smaller size due to the suppression of rainband formation (Figure S2) and
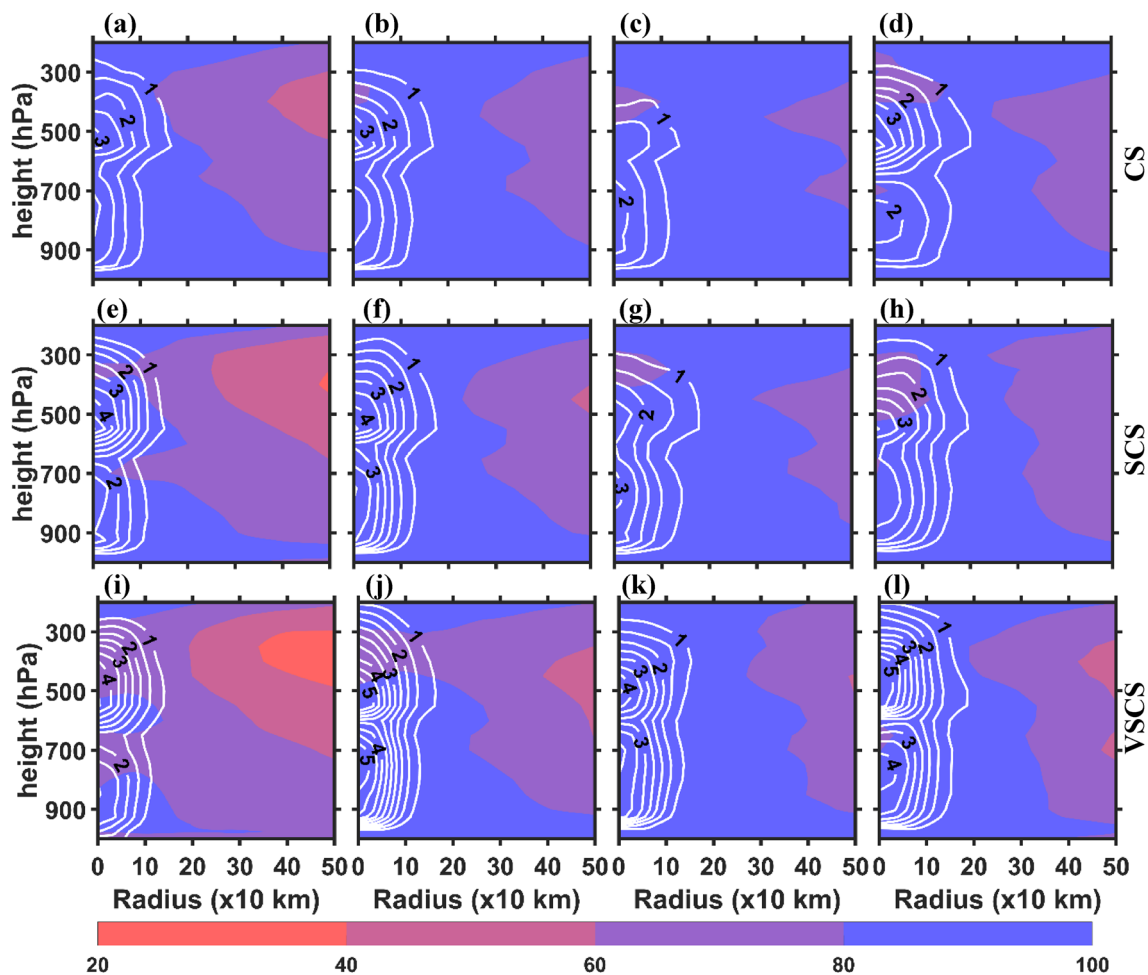
Fig. 9 Azimuthally averaged relative humidity (shading; %) and potential vorticity (contours; PVU = 10^6 K m^2 s^{-1} kg^{-1}) for **a** Group-1, **b** Group-2, **c** Group-3, and **d** Group-4 cyclones during at a cyclone (CS) intensity stage. **e–l** Are similar to **a–d** but for the SCS and VSCS stages

it supports the faster intensification of TC. Similar results were found in the idealized study of Ying and Zhang 2012.

The role of large-scale dynamical properties (i.e. wind shear) on the size-intensity relation is analyzed in supplementary Figure S3. The deep wind shear is calculated between the two atmospheric layers such as 850 and 200 hPa. Note that the wind shear is estimated within an 800 km storm radius and the inner core wind shear is filtered out. Results indicate that the wind shear increases from Group-1 to Group-4 for all intensity stages (Figure S2). Gao et al. (2020) demonstrated that the strong shear promotes the formation of rain-bands in the down shear side, which may aid to increase the TC size (Wang 2009).

4 Discussions and conclusion

The intensity and size of a tropical cyclone (TC) determine the degree/severity of destruction during the landfall process. The relationship between these two TC physical parameters is not well studied over the North Indian Ocean basin. This study aims to examine the relation between TC intensity and size parameters (such as radius of maximum wind (R_{max}) and radius of 34 knots wind field (R34)). In addition, a new metric for TC size known as TC fullness (TCF) which provides the areal expansion of the convective ring from the TC center is also analyzed.

The TC size metrics across the NIO basin show high variations, particularly in R34 size. For instance, R34 of 100–150 km is more frequent (10%) for the BoB TCs, while

it is 5% for AS TCs. The R_{max} typically varies between 20 to 60 km. The NIO TCs exhibit a bigger convective ring (TCF of 0.6 to 0.8) around the TC center at a higher frequency. It is assumed that the TC intensity plays a role in the uneven distribution of TC sizes. Intensity is found to have a relatively stronger correlation (0.7) with TCF when compared to that with R34 (0.5) and R_{max} (0.6) for all TC intensities. Note that the correlation between 12 h intensity and size changes is poor, varying between 0.37 and 0.39. It indicated that the size of TC does not monotonically increase with the intensity.

All the VSCS and above-intensity TCs are categorized into four groups to understand the causes that are responsible for poor relation between R34 and intensity. Group-1, Group-2, Group-3, and Group-4 TCs exhibit an average LRC of 1.42, 2.18, 2.7, and 3.7 km/knot, respectively between size and intensity. The average size of Group-1 TCs is about 100 km, and it is ~150, ~190, and ~240 km in Group-2 to Group-4, respectively. The majority of TCs (~50%) belong to Group-2 (i.e. size monochromatically increases with intensity), followed by Group-1 (25%) in which the size is almost similar for different intensities. The contribution of Group-3 (large size for smaller intensity changes) is 10% and Group-4 TCs having a larger size at initial time is 15%.

The analysis of surface and atmospheric conditions reveals the following facts that affect the relationship between TC size and intensity, and is summarized in Table 1.

1. In Group-1 TCs, the presence of dry air outside the eyewall region could be responsible for preventing the

Table 1 A summary of factors that are associated with various groups

Parameters	Group-1	Group-2	Group-3	Group-4
Character	Intensity increases and no/limited changes in size	Intensity and size increases	No/less change in intensity and increase in size	Initially larger vortex
Average LRC (R34 at VSCS stage)	1.42 km/knots (100 km)	2.18 km/knots (150 km)	2.7 km/knots (190 km)	3.7 km/knots (240 km)
Vortex (radial wind)	Narrower (low)	Well-defined (strong and narrower)	ill-defined (strong and wider)	ill-defined (strong and widest)
Vertical velocity (AAM)	Smaller in inner –core (less)	Strongest in inner-core (stronger in lower and upper levels)	Wider (lower in upper levels)	Wider (strongest in TC region)
Surface fluxes	Low and confined in inner-core	Strongest in inner-core	Wider	Wider and strong form initial time
RH (PV)	Dry air intrusion in the outer core region (narrower)	Relatively dry air in the environment (wider)	Humid environment (wider and weak PV in upper-levels)	Relative dry air in the environment (widest)
Impact	Suppress the rainband formation	Strong inner-core convection	Favorable to rainband or secondary eye wall formation	Large area of convection from initial period
References	Ying and Zhang (2012), Hill and Lackmann (2009)	Kilroy et al. (2016), Nekkali et al. (2022a)	Wang (2009), Hill and Lackmann (2009)	Xu and Wang (2010)

rain band development, thus limiting the size growth. In addition, low vertical wind shear supports the maintenance of TCs and helps strengthen the TC. Similar results are observed in the modeling study of Ying and Zhang (2012).

2. Substantial convection in the primary eyewall is supported by the strong surface fluxes near TC centers in Group-2. Strong convection and associated latent heat in the primary eyewall region enhance the angular momentum from lower to upper levels, which in turn encourages an increase in both size and intensity. Similar outcomes were found in the modeling study of Nekkali et al. (2022b).

3. A humid environment and strong and broader surface fluxes may create rain-bands or secondary-eyewall and hence increase the convection outside of the eyewall favoring the size to increase and limiting intensity (shows in terms of a weaker vortex and low upper lever potential vorticity). In addition, relatively strong/similar (Weak) AAM in the lower (upper) troposphere favors the TC size (limits the intensity). Similar results were found in the study of Wang (2009), Chan and Chan (2013).

4. The larger initial vortex sustains broader surface fluxes, vertical velocities, and strong AAM in the TC's inner and outer core areas. This increases the strength of the TC which significantly broadens the tangential wind to form broader convective/rain bands. Thus, the size maintains or increases in the lifetime of the Group-4 TCs and the results are consistent with previous studies (Xu and Wang 2010, 2018a). Further, Chan and Chan (2014) demonstrated that the TCs that are initially smaller in size might not remain as smaller throughout their lifetime, however, the larger TCs maintain or remain as larger TCs during their lifetime.

It is worthwhile to note that there could be uncertainties in the TC size and intensity relationships and mainly due to the limitations in the datasets such as ERA5 (Malakar et al. 2020) and IR brightness temperature data (Lu et al. 2017), and best track data (Ren et al. 2011). Further, the relationships can be reexamined by considering (i) high-resolution regional analyses or numerical model simulations (ii) microwave brightness temperatures, etc. to enhance the knowledge on the physical processes underpinning the relationship between size and intensity of TCs.

Declarations

References

Abarca SF, Montgomery MT (2013) Essential dynamics of secondary eyewall formation. J Atoms Sci 70(10):3216–3230

Ankur K, Busireddy NKR, Osuri KK, Niyogi D (2020) On the relationship between intensity changes and rainfall distribution in tropical cyclones over the North Indian Ocean. Int J Climatol 40(4):2015–2025

Balachandran S, Geetha B (2017) Diagnostics of upper level dynamics and rainfall asymmetry of very severe cyclonic storm MADI (2013). In: Tropical cyclone activity over the North Indian Ocean, pp 61–72

Busireddy NKR, Ankur K, Osuri KK, Sivareddy S, Niyogi D (2019) The response of ocean parameters to tropical cyclones in the Bay of Bengal. Q J R Meteorol Soc 145(724):3320–3332

Busireddy NKR, Ankur K, Osuri KK, Niyogi D (2022) Modelled impact of ocean warming on tropical cyclone size and destructiveness over the Bay of Bengal: a case study on FANI cyclone. Atmos Res 279:p106355

Chan KT, Chan JC (2013) Angular momentum transports and synoptic flow patterns associated with tropical cyclone size change. Mon Weather Rev 141(11):3985–4007

Chan KT, Chan JC (2014) Impacts of initial vortex size and planetary vorticity on tropical cyclone size. Q J R Meteorol Soc 140(684):2235–2248

Chan KT, Chan JC (2015) Impacts of vortex intensity and outer winds on tropical cyclone size. Q J R Meteorol Soc 141(687):525–537

Chan KT, Chan JC (2018) The outer-core wind structure of tropical cyclones. J Meteorol Soc Jpn Ser II 96(4):297–315

Chen K, Chen G, Rao C, Wang Z (2021) Relationship of tropical cyclone size change rate with size and intensity over the western North Pacific. Atmos Ocean Sci Lett 14(3):p100040

Gao Q, Li Q, Dai Y (2020) Characteristics of the outer rainband stratiform sector in numerically simulated tropical cyclones: lowerlayer shear versus upper-layer shear. Adv Atmos Sci 37:399–419

Guo X, Tan ZM (2017) Tropical cyclone fullness: a new concept for interpreting storm intensity. Geophys Res Lett 44(9):4324–4331

Hersbach H, Bell B, Berrisford P, Hirahara S, Horányi A, MuñozSabater J, Nicolas J, Peubey C, Radu R, Schepers D, Simmons A (2020) The ERA5 global reanalysis. Q J R Meteorol Soc 146(730):1999–2049

Hill KA, Lackmann GM (2009) Influence of environmental humidity on tropical cyclone size. Mon Weather Rev 137(10):3294–3315

Holland GJ, Merrill RT (1984) On the dynamics of tropical cyclone structural changes. Q J R Meteorol Soc 110(465):723–745

Huffman GJ, Stocker EF, Bolvin DT, Nelkin EJ, Tan J (2019) GPM IMERG final precipitation L3 half hourly 01 degree x 01 degree V06 In: Goddard Earth Sciences Data and Information Services Center (GES DISC): Greenbelt, MD, USA

Irish JL, Resio DT, Ratcliff JJ (2008) The influence of storm size on hurricane surge. J Phys Oceanogr 38(9):2003–2013

Kilroy G, Smith RK, Montgomery MT (2016) Why do model tropical cyclones grow progressively in size and decay in intensity after reaching maturity? J Atmos Sci 73(2):487–503

Knaff JA, Sampson CR, DeMaria M, Marchok TP, Gross JM, McAdie CJ (2007) Statistical tropical cyclone wind radii prediction using climatology and persistence. Weather Forecast 22(4):781–791

Knapp KR, Ansari S, Bain CL, Bourassa MA, Dickinson MJ, Funk C, Helms CN, Hennon CC, Holmes CD, Huffman GJ, Kossin JP (2011) Globally gridded satellite observations for climate studies. Bull Am Meteorol Soc 92(7):893–907

Li J, Hou Y, Mo D, Liu Q, Zhang Y (2019) Influence of tropical cyclone intensity and size on storm surge in the Northern East China Sea. Remote Sens 11(24):3033

Lin Y, Zhao M, Zhang M (2015) Tropical cyclone rainfall area controlled by relative sea surface temperature. Nat Commun 6(1):6591

Lu X, Yu H, Yang X, Li X (2017) Estimating tropical cyclone size in the Northwestern Pacific from geostationary satellite infrared images. Remote Sens 9(7):p728

Lyu X, Wang X, Leslie LM (2019) The dependence of Northwest Pacific tropical cyclone intensification rates on environmental factors. Adv Meteorol 2019:1–18

Ma Q, Li Y, Feng H, Yu Q, Zou Y, Liu F, Pulatov B (2021) Performance evaluation and correction of precipitation data using the 20-year IMERG and TMPA precipitation products in diverse sub-regions of China. Atmos Res 249:105304

Malakar P, Kesarkar AP, Bhate JN, Singh V, Deshamukhya A (2020) Comparison of reanalysis data sets to comprehend the evolution of tropical cyclones over North Indian Ocean. Earth Space Sci 7(2):pe2019EA000978

Meenu S, Rajeev K, Parameswaran K, Nair AKM (2010) Regional distribution of deep clouds and cloud top altitudes over the Indian subcontinent and the surrounding oceans. J Geophys Res 115:D05205. https://doi.org/10.1029/2009JD011802

Merrill RT (1984) A comparison of large and small tropical cyclones. Mon Weather Rev 112(7):1408–1418. https://doi.org/10.1175/1520-0493(1984)11220CO;2

Mohapatra M (2014) Tropical cyclone forecast verification by India Meteorological Department for north Indian Ocean: a review. Trop Cyclone Res Rev 3(4):229–242

Mohapatra M, Sharma M (2015) Characteristics of surface wind structure of tropical cyclones over the north Indian Ocean. J Earth Syst Sci 124:1573–1598

Nadimpalli R, Mohanty S, Pathak N, Osuri KK, Mohanty UC, Chatterjee S (2021) Understanding the characteristics of rapid intensity changes of Tropical Cyclones over North Indian Ocean. SN Appl Sci 3:1–12

Nadimpalli R, Nekkali S, Osuri K, Sil S, Das A (2023) Study of the impact of high resolution ROMS-SST on the simulation of two intense tropical cyclones over Bay of Bengal using ARW modeling system. Mausam 74(1):105–118

Nekkali YS, Osuri KK, Das AK (2022a) Numerical modeling of tropical cyclone size over the Bay of Bengal: influence of

microphysical processes and horizontal resolution. Meteorol Atmos Phys 134(4):72

Nekkali YS, Osuri KK, Das AK, Niyogi D (2022b) Understanding the characteristics of microphysical processes in the rapid intensity changes of tropical cyclones over the Bay of Bengal. Q J R Meteorol Soc 148(749):3715–3729

Qi F, Fei J, Ma Z, Chen J, Huang X, Cheng X (2018) Comparison of simulated tropical cyclone intensity and structures using the WRF with hydrostatic and nonhydrostatic dynamical cores. Atmosphere 9(12):p483

Qin N, Zhang DL, Li Y (2016) A statistical analysis of steady eyewall sizes associated with rapidly intensifying hurricanes. Weather Forecast 31(3):737–742

Ren F, Liang J, Wu G, Dong W, Yang X (2011) Reliability analysis of climate change of tropical cyclone activity over the western North Pacific. J Clim 24(22):5887–5898

Ruan Z, Wu Q (2022) Relationship between size and intensity in North Atlantic tropical cyclones with steady radii of maximum wind. Geophys Res Lett 49(3):pe2021GL095632

Saikrishna TS, Ramu DA, Osuri KK (2021) Inter-comparison of high-resolution satellite precipitation products over India during the summer monsoon season. Meteorol Atmos Phys 133:1675–1690

Shen LZ, Wu CC, Judt F (2021) The role of surface heat fluxes on the size of Typhoon Megi (2016). J Atmos Sci 78(4):1075–1093

Song J, Duan Y, Klotzbach PJ (2020) Revisiting the relationship between tropical cyclone size and intensity over the western North Pacific. Geophys Rese Lett 47(13):pe2020GL088217

Tao D, Zhang F (2019) Evolution of dynamic and thermodynamic structures before and during rapid intensification of tropical cyclones: Sensitivity to vertical wind shear. Mon Weather Rev 147(4):1171–1191

Wang Y (2009) How do outer spiral rainbands affect tropical cyclone structure and intensity? J Atmos Sci 66(5):1250–1273

Wu L, Tian W, Liu Q, Cao J, Knaff JA (2015) Implications of the observed relationship between tropical cyclone size and intensity over the western. North Pacific J Clim 28(24):9501–9506

Xu J, Wang Y (2010) Sensitivity of tropical cyclone inner-core size and intensity to the radial distribution of surface entropy flux. J Atmos Sci 67(6):1831–1852

Xu J, Wang Y (2018a) Effect of the initial vortex structure on intensification of a numerically simulated tropical cyclone. J Meteorol Soc Jpn Ser II 96(2):111–126

Xu J, Wang Y (2018b) Dependence of tropical cyclone intensification rate on sea surface temperature, storm intensity, and size in the western North Pacific. Weather Forecast 33(2):523–537

Ying Y, Zhang Q (2012) A modeling study on tropical cyclone structural changes in response to ambient moisture variations. J Meteorol Soc Jpn Ser II 90(5):755–770